frontiers | Frontiers in Neuroscience

TYPE Brief Research Report
PUBLISHED 10 September 2025
DOI 10.3389/fnins.2025.1665976

OPEN ACCESS

EDITED BY
Goichi Miyoshi,
Gunma University, Japan

REVIEWED BY
Takako Kikkawa,
Tohoku University Graduate School of Medicine, Japan
Anthony Rossi,
Department of Neurobiology and Harvard Medical School, United States

*CORRESPONDENCE
Euiseok J. Kim
ekim62@ucsc.edu

RECEIVED 14 July 2025
ACCEPTED 19 August 2025
PUBLISHED 10 September 2025

CITATION
Major M, Pham P, Hernandez-Alvarez E and Kim EJ (2025) Distinct neurogenic dynamics of cortico-cortical neuronal subtypes in layer 2/3 of the mouse visual cortex.
Front. Neurosci. 19:1665976.
doi: 10.3389/fnins.2025.1665976

Distinct neurogenic dynamics of cortico-cortical neuronal subtypes in layer 2/3 of the mouse visual cortex

Mustapha Major[1], Paul Pham[1], Efrain Hernandez-Alvarez[1] and Euiseok J. Kim[1,2]*

[1]Department of Molecular, Cell, and Developmental Biology, University of California, Santa Cruz, Santa Cruz, CA, United States, [2]Institute for the Biology of Stem Cells, University of California, Santa Cruz, Santa Cruz, CA, United States

In the mammalian cerebral cortex, the birthdates of excitatory projection neurons are closely linked to their laminar positions, which are often associated with distinct long-range projection targets. Although broad relationships between neurogenic timing, laminar position, and projection patterns are well established, the degree to which birthdate specifies projection identity within the same cortical layer remains unclear. In the mouse primary visual cortex (V1), neurons projecting to lateral higher visual areas are relatively evenly distributed throughout layer 2/3, whereas those projecting to medial areas are biased toward more superficial sublayers. To determine whether these projection identities are linked to neurogenic timing, we combined EdU birthdating with retrograde viral tracing. Notably, we found that V1 layer 2/3 neurons projecting to lateral higher visual areas are preferentially born at embryonic day 15.5 (E15.5) compared to E16.5, whereas V1 neurons projecting to medial higher visual areas show no significant birthdate bias between E15.5 and E16.5. These findings suggest that distinct cortico-cortical projection subtypes in layer 2/3 are generated on different temporal schedules, linking neurogenic timing to fine-scale projection identity.

KEYWORDS

neurogenesis, cortico-cortical projection neurons, L2/3 neurons, mouse visual cortex, birthdating, neuronal subtypes

Introduction

Understanding how diverse neuronal subtypes emerge during development is a central question in neurobiology. The mammalian brain consists of a wide array of cell types distinguished by morphology, molecular identity, physiology, connectivity, and anatomical location. Historically, neurons were classified by gross morphology and anatomical location (Glickstein, 2006; Nelson et al., 2006; Fishell and Heintz, 2013), but recent advances in transcriptomics and circuit mapping have enabled much finer classifications, revealing hierarchical taxonomies of neuronal types across the mouse brain (Tasic et al., 2016; Zeng and Sanes, 2017; Yao et al., 2021). Within these taxonomies, excitatory neurons in the neocortex are broadly classified into major projection classes such as intratelencephalic (IT or cortico-cortical projection neurons, CCPNs), extratelencephalic (ET), corticothalamic (CT), and near-projecting types based on their laminar position and long-range connectivity (Harris and Shepherd, 2015).

However, even within a single layer and projection class, further subclassification reveals considerable cellular diversity. For example, in layer 2/3 (L2/3) of the mouse primary visual

cortex (V1), CCPNs project to a variety of higher visual areas (HVAs) with specific projection motifs forming anatomical subtypes (Wang and Burkhalter, 2007; Han et al., 2018; Kim et al., 2020). Among these, neurons projecting to the anterolateral (AL) and posteromedial (PM) HVAs, L2/3 V1 → AL and L2/3 V1 → PM respectively, form largely non-overlapping groups with distinct properties. They differ in visual tuning preferences (Glickfeld et al., 2013) and local circuit connectivity (Kim et al., 2018), rarely co-project to both AL and PM (Kim et al., 2018, 2020), and receive selective long-range feedback predominantly from their respective target areas (Kim et al., 2020). These features support the notion that L2/3 CCPNs in V1 comprise discrete subtypes with distinct circuit identities.

One underexplored question is how these subtype-specific projection identities are developmentally specified. A clue may lie in their laminar positioning: L2/3 V1 → AL neurons are evenly distributed across L2/3, whereas L2/3 V1 → PM neurons are more superficial (Kim et al., 2018, 2020; Cheng et al., 2022; Han and Bonin, 2024). Since cortical neurons are generated in an inside-out sequence, with earlier-born neurons settling deeper and later-born neurons migrating to more superficial positions (Angevine and Sidman, 1961; McConnell, 1995; Rakic, 2007), we hypothesized that birthdate contributes to projection identity within L2/3.

To test this hypothesis, we asked whether V1 neurons projecting to lateral versus medial HVAs differ in their birth timing. We defined AL, rostrolateral (RL), and lateromedial (LM) as lateral HVAs (L-HVAs) and PM and anteromedial (AM) as medial HVAs (M-HVAs), based on their axonal projection targets (Figure 1A). To assess birthdate, we administered EdU at embryonic days E14.5, E15.5, or E16.5, and used fluorescently tagged AAVretro virus tracers to label V1 CCPNs projecting to either L-HVAs or M-HVAs. By comparing the birthdate distributions of these projection-defined populations, we determined whether distinct L2/3 CCPN subtypes arise at different developmental time points.

Methods

Experimental animals and husbandry

C57BL/6 J mice were used as wild-type. Both male and female mice were used. The specific ages and conditions of the experimental animals are described in Table 1. All mice were housed with a 12 h light and 12 h dark cycle and *ad libitum* access to food and water. All animal procedures were performed in accordance with the University of California, Santa Cruz animal care and use committee (IACUC)'s regulations.

EdU (5-ethynyl-2′-deoxyuridine) injection

Male and female wildtype mice were crossed to each other with a 12 h breeding window, and females were checked daily for vaginal plugs to determine date of conception. The time point at which a plug was detected was considered embryonic day (E) 0.5. Pregnant dams

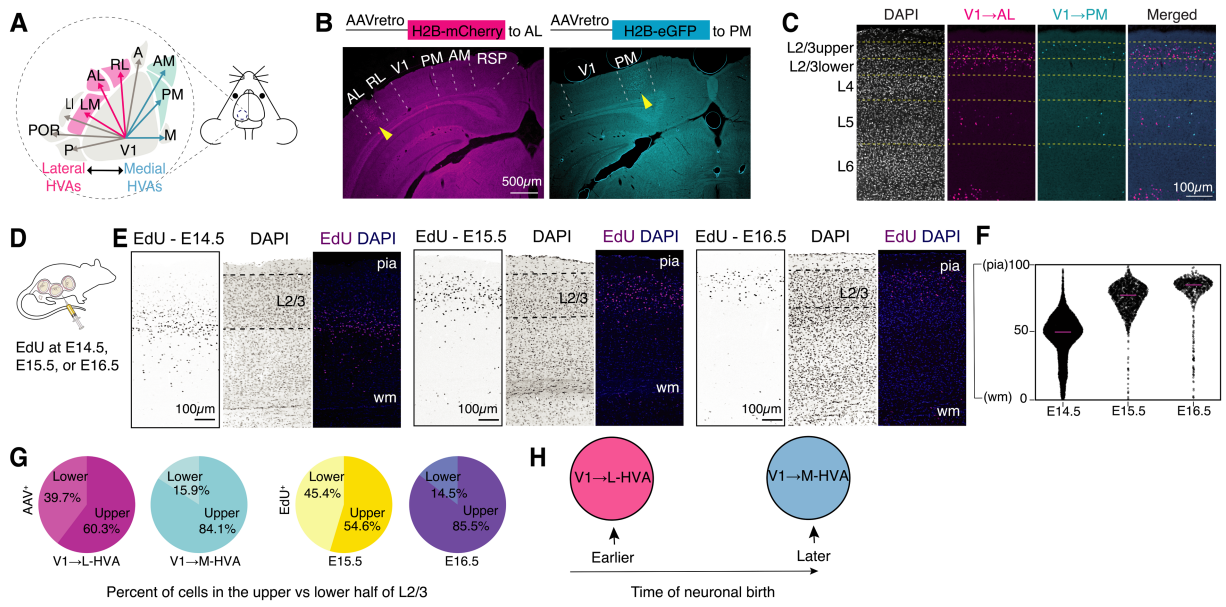

FIGURE 1
Differential laminar distribution of V1 neurons projecting to distinct higher visual areas (HVAs) and of EdU-labeled neurons from E14.5 to E16.5. **(A)** Schematic of primary visual cortex (V1) and surrounding HVAs. **(B)** Coronal sections showing representative retrograde labeling using AAVs injected into lateral (AL, left) and medial (PM, right) HVAs, with yellow arrowheads indicating the injection sites. **(C)** Example coronal images of AAVretro-labeled neurons in V1 following injections into AL (magenta) and PM (cyan). **(D)** Diagram illustrating the EdU labeling protocol during embryonic development. **(E)** Representative images of EdU-labeled cells in coronal V1 sections from mice injected at E14.5 (left), E15.5 (middle), or E16.5 (right) and analyzed in adulthood (P47 to P92). n = 6, n = 7, and n = 8 mice for the E14.5, E15.5, and E16.5 groups, respectively. **(F)** Violin plots showing the distribution of EdU+ cells along the cortical depth from pia to the white matter (wm) in three example adult mice across the whole primary visual cortex. Data are represented as median. **(G)** Pie charts illustrating the proportion of AAV+ (left) and EdU+ (right) neurons located in the upper versus lower half of V1 L2/3. Data are represented as mean. **(H)** Working model: L2/3 V1 neurons projecting to lateral HVAs (L-HVAs) are predominantly born earlier, whereas those projecting to medial HVAs (M-HVAs) are born later.

TABLE 1 Summary of animal information, experimental conditions, cell counts, and colocalization percentages.

Sample ID	EdU injection	AAV injection location	AAV	Age at injection	# of AAV$^+$ cells	# of EdU$^+$ cells	# of colocalized cells	Percent colocalized	Sex	Litter ID
S17	E14.5	AL	AAVretro-eGFP	P63	778	157	2	0.26	M	J
S18	E14.5	PM	AAVretro-mCherry	P63	401	491	4	1	M	J
S19	E14.5	PM	AAVretro-eGFP	P84	531	289	1	0.19	F	J
S20	E14.5	AL	AAVretro-mCherry	P88	1,058	483	4	0.38	M	K
S21	E14.5	PM	AAVretro-eGFP	P88	437	360	0	0	M	K
S22	E14.5	AL	AAVretro-mCherry	P69	99	135	0	0	F	G
S09	E15.5	AL	AAVretro-eGFP	P47	1912	1,503	289	15.12	M	P
S12	E15.5	AL	AAVretro-eGFP	P90	1,472	1,587	363	24.66	M	Q
S08	E15.5	LM	AAVretro-mCherry	P47	520	1893	178	34.23	M	P
S11	E15.5	LM	AAVretro-eGFP	P47	369	1,234	83	22.49	M	P
S10	E15.5	PM	AAVretro-mCherry	P47	288	966	29	10.07	M	P
S14	E15.5	AM	AAVretro-mCherry	P92	308	863	45	14.61	F	Q
S01	E15.5	AM	AAVretro-mCherry	P68	1,034	1906	170	16.44	M	E
S04	E16.5	AL	AAVretro-mCherry	P73	3,445	2,396	333	9.67	F	H
S05	E16.5	AL	AAVretro-mCherry	P73	456	895	35	7.68	F	H
S06	E16.5	AL	AAVretro-mCherry	P81	1,517	851	152	10.02	F	O
S03	E16.5	AL/RL	AAVretro-eGFP	P73	488	359	24	4.92	M	H
S07	E16.5	LM	AAVretro-eGFP	P81	1,275	1,616	91	7.14	F	H
S02	E16.5	PM	AAVretro-mCherry	P73	358	825	35	9.78	M	H
S15	E16.5	PM	AAVretro-mCherry	P81	189	514	28	14.81	F	R
S16	E16.5	PM/AM	AAVretro-mCherry	P85	483	978	79	16.36	F	S

were given one intraperitoneal (IP) injection of 25 mg/kg EdU (MilliporeSigma, 900584) at E14.5, E15.5, or E16.5.

Virus preparation and stereotaxic animal surgery

Adeno-associated virus (AAVs) were produced by the Salk Viral Core GT3: scAAVretro-hSyn-H2B-eGFP (referred to hereafter as AAVretro-eGFP, 1.16×10^{13} GC/ml), scAAVretro-hSyn-H2B-mCherry (referred to hereafter as AAVretro-mCherry, 1.21×10^{13} GC/ml).

Mice from postnatal day (P) 47 to P92 were used. Mice were anesthetized with an IP injection of a cocktail containing 80.4 mg/kg ketamine and 8 mg/kg xylazine cocktail, and continuous inhalation of 1–3% gaseous isoflurane throughout the procedure. To label V1 neurons projecting to AL, PM, and other HVAs, 15–50 nL of AAVretro-eGFP or AAVretro-mCherry was injected into the target HVA. The fluorescent protein used in the lateral or medial injection was alternated between each animal (see Table 1). Injection sites were located using stereotaxic coordinates relative to lambda on the mediolateral and anteroposterior axes, and relative to the pia on the dorsoventral axis: 3.5 mm lateral, 1–1.5 mm anterior, and 0.3 mm ventral for AL or L-HVAs; 1.6 mm lateral, 1.23–1.6 mm anterior, and 0.3–0.4 mm ventral for PM or M-HVAs. A drilled burr hole was made over the target area, and injections were done with a 20–30 µm diameter glass pipette, using air pressure from a 1 mL syringe with 18G tubing adapter and tubing. Post-surgery, 5 mg/kg of carprofen was injected intramuscularly, and mice were given water with ibuprofen (30 mg/kg).

Histology

Ten days after virus injection, mice underwent trans-cardiac perfusion using 1X phosphate-buffered saline (PBS) containing heparin (10 U/mL; Sigma-Aldrich, H3393) followed by 4% paraformaldehyde (PFA). Brains were dissected from skulls and postfixed with 2% PFA and 15% sucrose in PBS at 4 °C overnight and then immersed in 30% sucrose in 1X PBS at 4°C for a minimum of 24 h before sectioning. Using a sliding microtome (Espredia, HM430), 50 µm coronal brain sections were cut and stored in 1X PBS with 0.01% sodium azide or cryogen (3 parts ethylene glycol, 3 parts glycerol, 3 parts ddH_2O, 1 part 10x PBS) at 4°C. After washing 3 times, 10 min each with 1X PBS, EdU staining solution (100 mM Tris pH8.0, 4 mM CuSO4, 0.65 µM sulfo-Cy5 azide, 10 mM sodium ascorbate) was applied and incubated for 30 min at room temperature, protected from light. Sections were washed three times for 10 min each in 1X PBS, then incubated with DAPI (4′,6-diamidino-2-phenylindole; ThermoFisher Scientific Invitrogen, D1306) for 30 min at room temperature, protected from light. After an additional three washes in 1X PBS (10 min each), sections were mounted on slides using a polyvinyl alcohol mounting medium containing DABCO (PVA-DABCO) and allowed to air dry.

Imaging and quantification

Brain sections were imaged using a 4×/0.2 NA (wd: 20 mm) or a 10×/0.45 NA (wd: 4 mm) objective on a Keyence BZ-9000 microscope. For each animal, injection sites were evaluated to confirm that labeling was restricted to the appropriate cortical visual areas. Representative images were acquired using a Zeiss LSM 880 confocal microscope with either a 10×/0.45 NA (wd: 2.0 mm) or a 40×/0.95 NA corr (wd: 0.25 mm) objective. To quantify single- and double-labeled neurons in V1, cortical borders were delineated on each section based on the Allen mouse brain common coordinate framework reference atlas (Wang et al., 2020), and L2/3 was manually defined using the DAPI nuclear counterstain based on cell density. AAVretro-labeled neurons (AAV+) and double-labeled AAV+ EdU+ neurons were manually counted. Because EdU signal intensity is reduced by approximately 50% with each successive cell division (Pereira et al., 2017), the distribution of mean EdU+ signal intensities of individual neurons within each ROI was plotted, and a 50% cutoff relative to the brightest EdU+ cell was applied. This threshold, approximating the median EdU intensity, was used to identify neurons likely born near the time of EdU injection. Single-labeled EdU+ neurons were automatically detected using QuPath (Bankhead et al., 2017) and custom scripts applying the same intensity threshold.

Statistical analysis

p-values were calculated using one-way ANOVA with Tukey's HSD *post hoc* test, the Kruskal–Wallis test, or the Pearson correlation test with Python 3.12, depending on the distribution and characteristics of the data. Normality and equality of variance were assessed prior to statistical testing using the Shapiro–Wilk and Levene's test, respectively.

Results

To examine the sublaminar distribution of L2/3 CCPNs targeting medial (e.g., AM or PM) versus lateral (e.g., AL, LM, or RL) higher visual areas (HVAs) in the adult mouse cortex (P47–P92), we injected AAVretro-eGFP or AAVretro-mCherry into medial or lateral HVAs. Brain tissue was collected 10 days post-injection for analysis (Figures 1A,B). Coronal brain sections containing the visual cortex were assessed using the Allen mouse brain common coordinate framework to confirm accurate targeting of the retrograde AAVs to higher visual areas (Figure 1B) (Wang et al., 2020). Fluorescence imaging revealed that V1 CCPNs projecting to lateral and medial visual areas were differentially distributed within L2/3. Specifically, PM- or AM-projecting V1 CCPNs (V1 → M-HVAs) were concentrated at 28.19 ± 2.61% of the normalized depth within layer 2/3, measured from the top of the layer. In contrast, AL-, RL- or LM-projecting V1 CCPNs (V1 → L-HVAs) were more evenly distributed through the depth of L2/3 with an average depth of 43.59 ± 1.34% (Figure 1C). This distribution pattern aligns with previous reports (Kim et al., 2018, 2020; Han and Bonin, 2024), including those utilizing alternative retrograde tracers such as cholera toxin subunit B (Kim et al., 2020).

L2/3 neurons in the mouse cortex are predominantly generated between embryonic days (E) 14.5 and 16.5 (Vitali et al., 2018; Baumann et al., 2025). To assess neuronal birthdates within the visual cortex, we administered EdU, a thymidine analog, to pregnant dams at E14.5, E15.5, or E16.5 (Figure 1D). Although some EdU+ cells labeled at E14.5 were detected in L2/3, the majority localized to layer 4 (Figures 1E,F). In contrast, EdU+ cells labeled at E15.5 and E16.5 were abundantly present in L2/3 (Figures 1E–G). Among these, cells labeled at E15.5 were positioned significantly deeper from the pial surface than those labeled at E16.5 (48.10 ± 2.49%, 27.38 ± 1.73%, Figure 2).

We further quantified the proportion of neurons located in the upper versus lower half of L2/3. 39.68% of V1 → L-HVA CCPNs resided in the lower half, compared to only 15.90% of V1 → M-HVA CCPNs. Likewise, 45.35% of E15.5-born neurons were located in the lower half of the layer, while only 14.50% of E16.5-born neurons showed similar positioning (Figures 1G, 2). Both the mean and median soma depths were deeper for V1 → L-HVA neurons (mean: 43.59%, median: 41.77%) than for V1 → M-HVA neurons (mean: 28.19%, median: 23.59%), a pattern also reflected in the E15.5 (mean: 48.10%, median: 46.49%) versus E16.5 (mean: 27.38%, median: 22.66%) groups (Figure 2). This pattern was consistent among all individual samples with the exception of sample ID S01, which exhibited an EdU+ distribution that was intermediate to stereotyped E14.5 and E15.5 distribution patterns (Figure 2B).

Given the resemblance between the soma distribution of AL- or laterally projecting V1 CCPNs and that of E15.5-born L2/3 neurons, and between PM- or medially projecting V1 CCPNs and E16.5-born L2/3 neurons, we hypothesized that laterally projecting V1 CCPNs are predominantly generated at E15.5, whereas medially projecting CCPNs originate mostly at E16.5 (Figure 1H). To test this, we quantified the proportion of EdU+ neurons among AAVretro-labeled laterally or medially projecting V1 CCPNs within L2/3 across the entire V1 (Figure 3). For labeled V1 → L-HVA CCPNs, the percentage of EdU+ neurons was significantly higher in the E15.5 group than in the E16.5 group (24.12 ± 3.94% and 7.89 ± 0.92%, respectively; one-way ANOVA with Tukey's HSD *post hoc* test, $p = 0.0017$; Figure 3B), supporting our hypothesis. This trend remained consistent in animals with AAVretro injections specifically targeted to AL. In contrast, for V1 → M-HVA CCPNs, no significant difference in colocalization was observed between the E15.5 and E16.5 groups (13.71 ± 1.89% and 13.65 ± 1.99% respectively; one-way ANOVA with Tukey's HSD post hoc test, $p = 0.9997$; Figure 3B). As expected, EdU incorporation at E14.5 resulted in nearly zero colocalization with AAVretro-labeled CCPNs, regardless of projection target, reflecting the low number of E14.5-born neurons in L2/3 (Figure 3B).

To determine whether AAV and EdU colocalization rates were influenced by the spatial location of AAVretro injection sites, we analyzed the relationship between colocalization percentages and the medial–lateral and anterior–posterior coordinates of injection centers relative to bregma (Figure 3C). For lateral injections, there was a slight negative trend between colocalization percentage and distance from both the midline and anterior visual cortex; however, these correlations were not statistically significant ($p = 0.225$ for distance from both the midline and bregma, $p = 0.301$ for distance from the midline alone, and $p = 0.800$ for distance from the bregma alone; Pearson correlation test, Figure 3C). Similarly, no significant

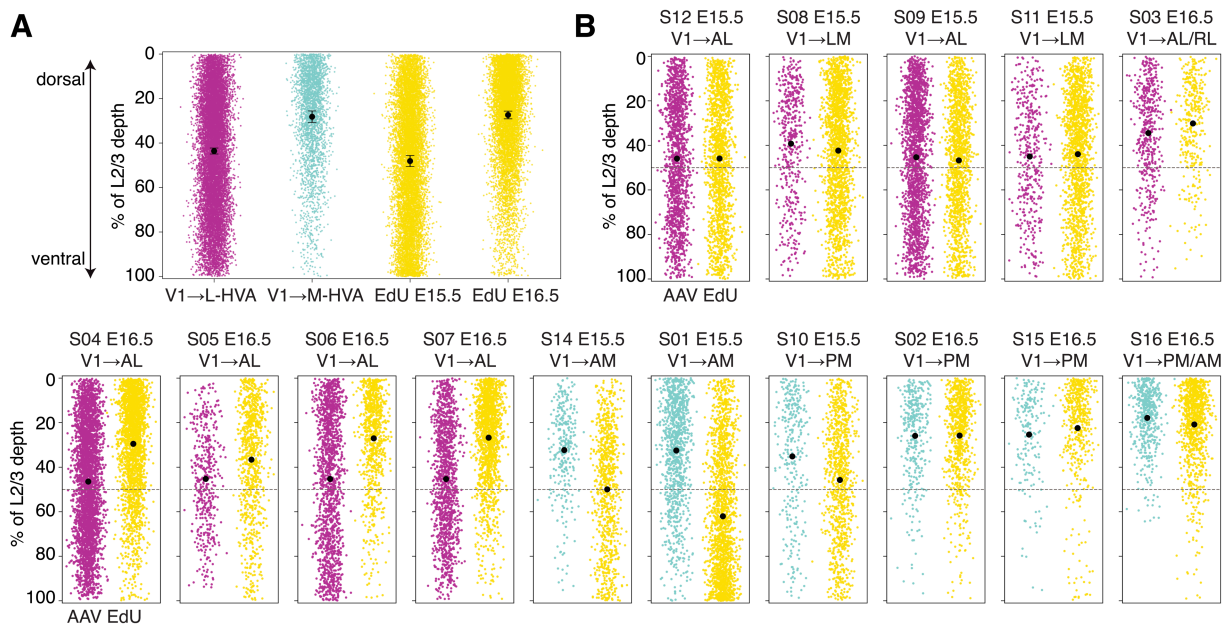

FIGURE 2
Sublaminar positioning of L2/3 V1 → L-HVA and V1 → M-HVA neurons parallels the laminar distributions of neurons born at E15.5 and E16.5. **(A)** Scatter plots showing the distribution of soma depth for AAV-labeled and EdU-labeled cells, measured relative to the dorsal boundary of layer 2 (0%) and the ventral boundary of layer 3 (100%). Black points indicate mean and error bars indicate SEM. **(B)** Scatter plots showing the soma depth distributions of individual AAV+ and EdU+ cells from samples S01–S16 (see Table 1 for details), aligned to the same reference points as in **(A)**. The dashed line indicates the midpoint of L2/3 depth.

correlation was observed between colocalization percentage and spatial coordinates for medial injections ($p = 0.966$ for distance from both the midline and bregma, $p = 0.849$ for distance from the midline alone, and $p = 0.879$ for distance from the bregma alone, Figure 3C). To determine whether the percentage of AAV and EdU colocalization was influenced by EdU+ cell density or laminar position within L2/3, we divided the full depth of L2/3 into ten equally spaced bins and quantified the proportion of AAV+ EdU+ neurons in each bin, normalized to the local EdU+ cell density (Figure 3D). This analysis was performed across all four experimental groups. We found no statistically significant differences in the distribution of colocalization percentages along the L2/3 depth in any of the groups. These results suggest that differences or similarities in AAV+ EdU+ colocalization rates between animal groups are not driven by confounding factors such as injection site location, EdU labeling density, or cortical depth.

Discussion

In summary, using a combination of birthdating and retrograde labeling, we found that L2/3 V1 → L-HVA neurons are preferentially generated at E15.5, with reduced production at E16.5, whereas L2/3 V1 → M-HVA neurons are generated at similar rates across both time points. These findings indicate a temporally biased wave of neurogenesis for L-HVA-projecting neurons, in contrast to a more uniform generation of M-HVA-projecting neurons (Figure 3E).

L2/3 CCPNs display considerable diversity in gene expression, local and long-range connectivity, and functional roles (Tasic et al., 2016; Meng et al., 2017; Kim et al., 2018, 2020; Yao et al., 2021). Our data reveal temporal differences in the birth rates of V1 CCPN subtypes. However, neuronal birthdate alone does not appear to dictate projection identity, as L2/3 CCPNs generated at the same embryonic stage can project to different targets. Additionally, although the somata of V1 → PM CCPNs are enriched in the upper portion of layer 2/3, their co-localization with EdU labeled at E15.5 or E16.5 is comparable (Figure 3B). This occurs despite the observation that E16.5-born neurons are positioned closer to the pial surface than E15.5-born neurons (Figure 1F). These findings suggest that the mechanisms guiding axonal targeting may be distinct from those regulating soma positioning, which may more directly reflect neuronal birthdate. While L2/3 V1 → M-HVA and V1 → L-HVA CCPNs exhibit divergent neurogenic patterns, birthdate alone may not fully account for their subtype identity, including differences in laminar distribution. Supporting this interpretation, recent findings by Huilgol et al. (2025) indicate that the corticogenesis of certain neuronal subtypes may diverge from the classical inside-out pattern typically associated with birthdate, highlighting additional complexity in cortical development (Huilgol et al., 2025). This raises the question of how discrete yet temporally close waves of neurogenesis give rise to such heterogeneous subtypes. In V1, the diversity among L2/3 CCPNs projecting to higher visual areas (HVAs) may stem from differences in progenitor origin: for example, direct versus indirect neurogenesis from radial glia or intermediate progenitors (Ellender et al., 2019; Huilgol et al., 2023). Alternatively, this heterogeneity could reflect depth-dependent, continuous changes in transcriptional programs that govern cell-type specification during cortical development (Cheng et al., 2022; Xie et al., 2025), consistent with the birthdate-dependent inside-out pattern of laminar organization. More specifically, cell recognition molecules involved in axon guidance and connectivity, such as *Cdh12/13*, *Cntn2/5*, *Epha3/6*, *Sema4a/6a*, and

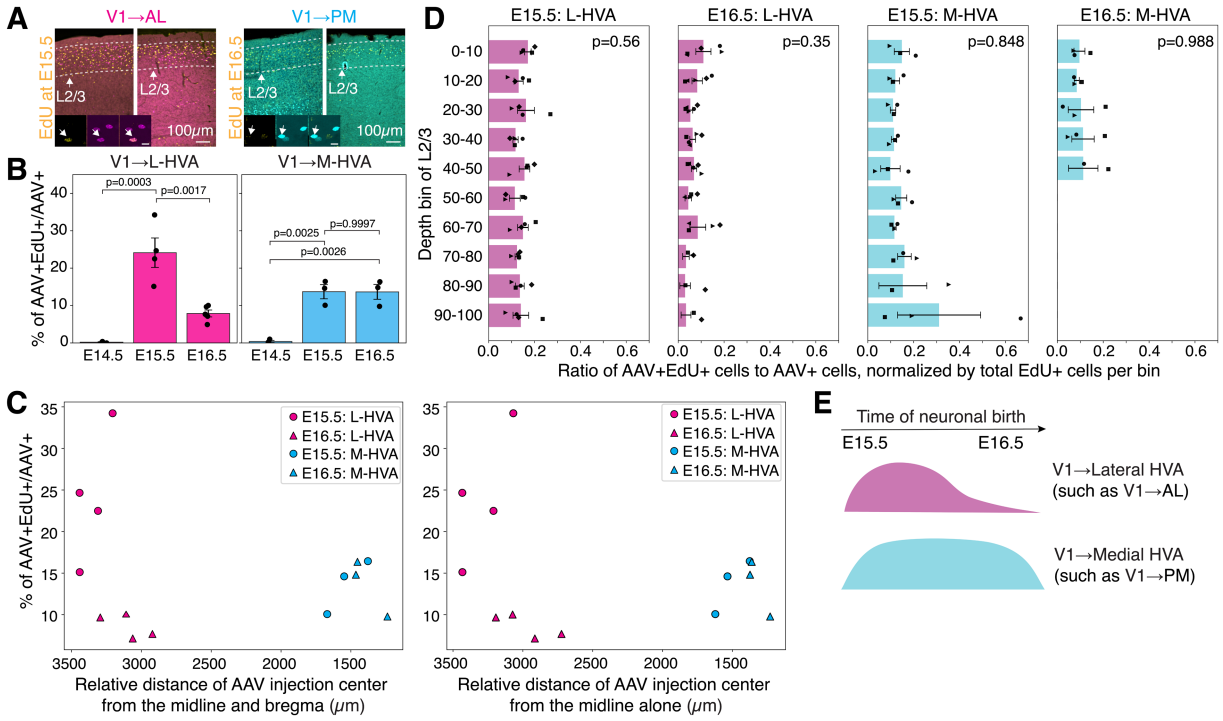

FIGURE 3
L2/3 V1 → L-HVA neurons are born in a greater proportion at E15.5 than at E16.5, while L2/3 V1 → M-HVA neurons show no temporal bias. **(A)** Fluorescent images of coronal sections of adult V1 showing AAV-labeled neurons projecting to AL (V1 → AL, magenta) and PM (V1 → PM, cyan), along with EdU+ neurons labeled at E15.5 or E16.5 (yellow). Insets display representative high-magnification images of strongly (left) and weakly (right) labeled AAV+ EdU+ cells. Arrows in insets indicate neurons with colocalized AAV and EdU signals. Scale bar (inset): 10 μm. **(B)** Percentage of AAV+ cells that are also EdU+ at E14.5, E15.5, or E16.5 in animals injected with AAVretro in a lateral HVA (left) or medial HVA (right). Each dot represents an individual animal. One-way ANOVA with Tukey's HSD *post hoc* tests. **(C)** Colocalization percentage is plotted against the distance of the AAVretro injection site from the midline and anterior position of the brain (left), or from the midline alone (right). **(D)** Normalized laminar distribution of AAV+ EdU+ neurons across L2/3 for each injection group. Kruskal-Wallis test. **(E)** Model summarizing temporally distinct neurogenesis of V1 L2/3 cortico-cortical projection neurons targeting lateral versus medial HVAs. n = 3 for E14.5 L-HVA, n = 3 for E14.5 M-HVA, n = 4 for E15.5 L-HVA, n = 3 for E15.5 M-HVA, n = 5 (except n = 4 in **C**) for E16.5 L-HVA, and n = 3 for E16.5 M-HVA. Data are represented as mean ± SEM.

Robo1, are differentially expressed across L2/3 subtypes distributed along the laminar depth (Cheng et al., 2022; Xie et al., 2025). Whether these molecular pathways contribute to subtype specification linked to projection identity remains an open question. Xie et al. (2025) also showed that visual deprivation alters both gene expression and cell type composition in V1 L2/3, suggesting that activity-dependent mechanisms may further influence the specification of projection-specific subtypes. This represents an important direction for future research.

Our study has several limitations. First, EdU-based birthdating provides relatively coarse temporal resolution, making it difficult to precisely determine the exact timing of neuronal birthdates (Landy et al., 2021). Mice were bred using a 12 h mating window, with the time of plug detection designated as E0.5, introducing a potential 12 h variability in labeling across animals. Although the spatial distribution of EdU+ cells labeled at E14.5, E15.5, and E16.5 was generally consistent across litters, one animal (sample ID S01) showed an intermediate distribution between typical E14.5 and E15.5 patterns (Figure 2B; Table 1), likely reflecting this variability. Additionally, because EdU is bioavailable for only 1–3 h after injection, it is unlikely that we captured the full cohort of neurons born on each labeling day during the neurogenic period of L2/3 neurons (Hayes and Nowakowski, 2000). To achieve finer resolution in birthdating, FlashTag, a cell-permeable fluorescent dye that labels M-phase apical progenitors, has been developed and applied to track neuron birthdates with greater precision (Govindan et al., 2018). This method has enabled detailed fate mapping, including downstream applications such as next-generation sequencing (Telley et al., 2019; Magrinelli et al., 2022), and may serve as a valuable tool for future studies. Nevertheless, we mitigated this potential limitation by analyzing multiple animals from independent breeders and litters, and by applying stringent criteria to identify birthdated neurons, selecting EdU+ cells that incorporated the label during their final S-phase before exiting the cell cycle on the day of EdU administration (See Methods). Second, retrograde labeling methods reveal only projections to the injected target site and do not capture the full extent of a neuron's axonal arborization (Han et al., 2018; Winnubst et al., 2019). Consequently, the complete projection patterns of CCPNs were not mapped in this study, and a comprehensive analysis linking birthdate to full projection identity remains to be conducted.

Building on the current findings, future studies using complementary approaches may help clarify how birth timing contributes to the development of L2/3 neurons with distinct

projection identities. One promising strategy is genetic birthdating using transgenic mouse lines that allow permanent labeling of neurons born at specific embryonic stages. For instance, inducible CreER lines such as Neurog1-CreER, Neurog2-CreER, or Tbr2-CreER, crossed with a Cre-dependent Flp-expressing reporter (e.g., loxP-STOP-loxP-Flp), can be used in combination with tamoxifen administration at defined embryonic time points (Kim et al., 2011; Hirata et al., 2021; Matho et al., 2021). In adult offspring, a Flp-dependent viral tracer such as AAV-fDIO (or FLEx^{frt})-fluorescent protein can be injected into V1 to selectively label axons of neurons born at those time points. This approach would enable direct quantification of V1 CCPN axons in medial versus lateral HVAs, allowing comparisons between early- and late-born L2/3 neurons. This strategy would enable testing whether early versus late birthdating of L2/3 CCPNs is broadly associated with distinct V1 projection patterns across the medial-lateral axis of higher visual areas. In parallel, transcriptomic or epigenomic profiling of these developmentally tagged neurons could uncover molecular mechanisms underlying subtype specification and projection identity (Isshiki et al., 2001; Molyneaux et al., 2007; Greig et al., 2013; Cheng et al., 2022). An important question for future investigation is whether similar temporal patterns of neurogenesis are observed in CCPNs of other cortical areas. For example, L2/3 CCPNs in the secondary visual cortex projecting to other HVAs, or those in the primary somatosensory or auditory cortices projecting to secondary cortical regions (Yamashita et al., 2018; Liu et al., 2019).

Data availability statement

The original contributions presented in the study are included in the article/supplementary material, further inquiries can be directed to the corresponding author.

Ethics statement

The animal study was approved by the University of California, Santa Cruz animal care and use committee (IACUC). The study was conducted in accordance with the local legislation and institutional requirements.

Author contributions

MM: Investigation, Visualization, Writing – original draft, Writing – review & editing, Data curation, Formal analysis, Methodology, Validation. PP: Data curation, Formal analysis, Investigation, Methodology, Writing – review & editing. EH-A: Data curation, Investigation, Methodology, Writing – review & editing. EK: Investigation, Writing – review & editing, Conceptualization, Funding acquisition, Resources, Supervision, Visualization, Writing – original draft.

Funding

The author(s) declare that financial support was received for the research and/or publication of this article. We acknowledge support from the UCSC start-up fund, the Whitehall Foundation, the Hellman Fellows Program, the E. Matilda Ziegler Foundation for the Blind, BRAIN Initiative at the National Institutes of Health RF1MH132591, the National Institute of Neurological Disorders and Stroke at the National Institutes of Health R01NS128771. The content is solely the responsibility of the authors and does not necessarily represent the official views of the National Institutes of Health.

Acknowledgments

We thank Bin Chen, Bradley Colquitt, Richard Dickson, and Matthew Jacobs for reading the manuscript. We acknowledge technical support from Benjamin Abrams, UCSC Life Sciences Microscopy Center, RRID: SCR_021135. Purchase of the Zeiss 880 confocal microscope used in this research was made possible through the National Institutes of Health s10 Grant 1S10OD23528-01. The illustration in Figure 1D was adapted from images provided by the NIAID NIH BioArt collection (bioart.niaid.nih.gov/bioart/506 and bioart.niaid.nih.gov/bioart/588).

Conflict of interest

The authors declare that the research was conducted in the absence of any commercial or financial relationships that could be construed as a potential conflict of interest.

Generative AI statement

The author(s) declare that Gen AI was used in the creation of this manuscript. Portions of the text in this manuscript were edited solely for clarity and grammar using ChatGPT (GPT-4 Turbo, OpenAI); no content or scientific interpretation was generated by the language model.

Any alternative text (alt text) provided alongside figures in this article has been generated by Frontiers with the support of artificial intelligence and reasonable efforts have been made to ensure accuracy, including review by the authors wherever possible. If you identify any issues, please contact us.

Publisher's note

References

Angevine, J. B., and Sidman, R. L. (1961). Autoradiographic study of cell migration during histogenesis of cerebral cortex in the mouse. *Nature* 192, 766–768. doi: 10.1038/192766b0

Bankhead, P., Loughrey, M. B., Fernández, J. A., Dombrowski, Y., McArt, D. G., Dunne, P. D., et al. (2017). QuPath: open source software for digital pathology image analysis. *Sci. Rep.* 7:16878. doi: 10.1038/s41598-017-17204-5

Baumann, N., Wagener, R. J., Javed, A., Conti, E., Abe, P., Lopes, A., et al. (2025). Regional differences in progenitor metabolism shape brain growth during development. *Cell* 188, 3567–3582.e20. doi: 10.1016/j.cell.2025.04.003

Cheng, S., Butrus, S., Tan, L., Xu, R., Sagireddy, S., Trachtenberg, J. T., et al. (2022). Vision-dependent specification of cell types and function in the developing cortex. *Cell* 185, 311–327.e24. doi: 10.1016/j.cell.2021.12.022

Ellender, T. J., Avery, S. V., Mahfooz, K., Scaber, J., von Klemperer, A., Nixon, S. L., et al. (2019). Embryonic progenitor pools generate diversity in fine-scale excitatory cortical subnetworks. *Nat. Commun.* 10:5224. doi: 10.1038/s41467-019-13206-1

Fishell, G., and Heintz, N. (2013). The neuron identity problem: form meets function. *Neuron* 80, 602–612. doi: 10.1016/j.neuron.2013.10.035

Glickfeld, L. L., Andermann, M. L., Bonin, V., and Reid, R. C. (2013). Cortico-cortical projections in mouse visual cortex are functionally target specific. *Nat. Neurosci.* 16, 219–226. doi: 10.1038/nn.3300

Glickstein, M. (2006). Golgi and Cajal: the neuron doctrine and the 100th anniversary of the 1906 Nobel prize. *Curr. Biol.* 16, R147–R151. doi: 10.1016/j.cub.2006.02.053

Greig, L. C., Woodworth, M. B., Galazo, M. J., Padmanabhan, H., and Macklis, J. D. (2013). Molecular logic of neocortical projection neuron specification, development and diversity. *Nat. Rev. Neurosci.* 14, 755–769. doi: 10.1038/nrn3586

Govindan, S., Oberst, P., and Jabaudon, D. (2018). In vivo pulse labeling of isochronic cohorts of cells in the central nervous system using FlashTag. *Nat Protoc*, 13, 2297–2311. doi: 10.1038/s41596-018-0038-1

Han, X., and Bonin, V. (2024). Higher-order cortical and thalamic pathways shape visual processing streams in the mouse cortex. *Curr. Biol.* 34, 5671–5684.e6. doi: 10.1016/j.cub.2024.10.048

Han, Y., Kebschull, J. M., Campbell, R. A. A., Cowan, D., Imhof, F., Zador, A. M., et al. (2018). The logic of single-cell projections from visual cortex. *Nature* 556, 51–56. doi: 10.1038/nature26159

Harris, K. D., and Shepherd, G. M. G. (2015). The neocortical circuit: themes and variations. *Nat. Neurosci.* 18, 170–181. doi: 10.1038/nn.3917

Hayes, N. L., and Nowakowski, R. S. (2000). Exploiting the dynamics of S-phase tracers in developing brain: interkinetic nuclear migration for cells entering versus leaving the S-phase. *Dev. Neurosci.* 22, 44–55. doi: 10.1159/000017426

Hirata, T., Tohsato, Y., Itoga, H., Shioi, G., Kiyonari, H., Oka, S., et al. (2021). NeuroGT: a brain atlas of neurogenic tagging CreER drivers for birthdate-based classification and manipulation of mouse neurons. *Cell Rep. Methods* 1:100012. doi: 10.1016/j.crmeth.2021.100012

Huilgol, D., Levine, J. M., Galbavy, W., Wang, B.-S., He, M., Suryanarayana, S. M., et al. (2023). Direct and indirect neurogenesis generate a mosaic of distinct glutamatergic projection neuron types in cerebral cortex. *Neuron* 111, 2557–2569.e4. doi: 10.1016/j.neuron.2023.05.021

Huilgol, D., Levine, J. M., Galbavy, W., Wang, B.-S., and Huang, Z. J. (2025). Orderly specification and precise laminar deployment of mouse cortical projection neuron types through intermediate progenitors. *Dev. Cell* 60, 1947–1957.e3. doi: 10.1016/j.devcel.2025.02.009

Isshiki, T., Pearson, B., Holbrook, S., and Doe, C. Q. (2001). Drosophila neuroblasts sequentially express transcription factors which specify the temporal identity of their neuronal progeny. *Cell* 106, 511–521. doi: 10.1016/s0092-8674(01)00465-2

Kim, E. J., Hori, K., Wyckoff, A., Dickel, L. K., Koundakjian, E. J., Goodrich, L. V., et al. (2011). Spatiotemporal fate map of neurogenin1 (Neurog1) lineages in the mouse central nervous system. *J. Comp. Neurol.* 519, 1355–1370. doi: 10.1002/cne.22574

Kim, E. J., Zhang, Z., Huang, L., Ito-Cole, T., Jacobs, M. W., Juavinett, A. L., et al. (2020). Extraction of distinct neuronal cell types from within a genetically continuous population. *Neuron* 107, 274–282.e6. doi: 10.1016/j.neuron.2020.04.018

Kim, M.-H., Znamenskiy, P., Iacaruso, M. F., and Mrsic-Flogel, T. D. (2018). Segregated subnetworks of Intracortical projection neurons in primary visual cortex. *Neuron* 100, 1313–1321.e6. doi: 10.1016/j.neuron.2018.10.023

Landy, M. A., Goyal, M., and Lai, H. C. (2021). Nociceptor subtypes are born continuously over DRG development. *Dev. Biol.* 479, 91–98. doi: 10.1016/j.ydbio.2021.07.018

Liu, J., Whiteway, M. R., Sheikhattar, A., Butts, D. A., Babadi, B., and Kanold, P. O. (2019). Parallel processing of sound dynamics across mouse auditory cortex via spatially patterned thalamic inputs and distinct areal intracortical circuits. *Cell Rep.* 27, 872–885.e7. doi: 10.1016/j.celrep.2019.03.069

Magrinelli, E., Baumann, N., Wagener, R. J., Glangetas, C., Bellone, C., Jabaudon, D., et al. (2022). Heterogeneous fates of simultaneously-born neurons in the cortical ventricular zone. *Sci. Rep.* 12:6022. doi: 10.1038/s41598-022-09740-6

Matho, K. S., Huilgol, D., Galbavy, W., He, M., Kim, G., An, X., et al. (2021). Genetic dissection of the glutamatergic neuron system in cerebral cortex. *Nature* 598, 182–187. doi: 10.1038/s41586-021-03955-9

McConnell, S. K. (1995). Constructing the cerebral cortex: neurogenesis and fate determination. *Neuron* 15, 761–768. doi: 10.1016/0896-6273(95)90168-x

Meng, X., Winkowski, D. E., Kao, J. P. Y., and Kanold, P. O. (2017). Sublaminar subdivision of mouse auditory cortex layer 2/3 based on functional translaminar connections. *J. Neurosci.* 37, 10200–10214. doi: 10.1523/JNEUROSCI.1361-17.2017

Molyneaux, B. J., Arlotta, P., Menezes, J. R. L., and Macklis, J. D. (2007). Neuronal subtype specification in the cerebral cortex. *Nat. Rev. Neurosci.* 8, 427–437. doi: 10.1038/nrn2151

Nelson, S. B., Sugino, K., and Hempel, C. M. (2006). The problem of neuronal cell types: a physiological genomics approach. *Trends Neurosci.* 29, 339–345. doi: 10.1016/j.tins.2006.05.004

Pereira, P. D., Serra-Caetano, A., Cabrita, M., Bekman, E., Braga, J., Rino, J., et al. (2017). Quantification of cell cycle kinetics by EdU (5-ethynyl-2′-deoxyuridine)-coupled-fluorescence-intensity analysis. *Oncotarget* 8, 40514–40532. doi: 10.18632/oncotarget.17121

Rakic, P. (2007). The radial edifice of cortical architecture: from neuronal silhouettes to genetic engineering. *Brain Res. Rev.* 55, 204–219. doi: 10.1016/j.brainresrev.2007.02.010

Tasic, B., Menon, V., Nguyen, T. N., Kim, T. K., Jarsky, T., Yao, Z., et al. (2016). Adult mouse cortical cell taxonomy revealed by single cell transcriptomics. *Nat. Neurosci.* 19, 335–346. doi: 10.1038/nn.4216

Telley, L., Agirman, G., Prados, J., Amberg, N., Fièvre, S., Oberst, P., et al. (2019). Temporal patterning of apical progenitors and their daughter neurons in the developing neocortex. *Science* 364:eaav2522. doi: 10.1126/science.aav2522

Vitali, I., Fièvre, S., Telley, L., Oberst, P., Bariselli, S., Frangeul, L., et al. (2018). Progenitor hyperpolarization regulates the sequential generation of neuronal subtypes in the developing neocortex. *Cell* 174, 1264–1276.e15. doi: 10.1016/j.cell.2018.06.036

Wang, Q., and Burkhalter, A. (2007). Area map of mouse visual cortex. *J. Comp. Neurol.* 502, 339–357. doi: 10.1002/cne.21286

Wang, Q., Ding, S.-L., Li, Y., Royall, J., Feng, D., Lesnar, P., et al. (2020). The Allen mouse brain common coordinate framework: a 3D reference atlas. *Cell* 181, 936–953.e20. doi: 10.1016/j.cell.2020.04.007

Winnubst, J., Bas, E., Ferreira, T. A., Wu, Z., Economo, M. N., Edson, P., et al. (2019). Reconstruction of 1,000 projection neurons reveals new cell types and organization of long-range connectivity in the mouse brain. *Cell* 179, 268–281.e13. doi: 10.1016/j.cell.2019.07.042

Xie, F., Jain, S., Xu, R., Butrus, S., Tan, Z., Xu, X., et al. (2025). Spatial profiling of the interplay between cell type- and vision-dependent transcriptomic programs in the visual cortex. *Proc. Natl. Acad. Sci. USA* 122:e2421022122. doi: 10.1073/pnas.2421022122

Yamashita, T., Vavladeli, A., Pala, A., Galan, K., Crochet, S., Petersen, S. S. A., et al. (2018). Diverse long-range axonal projections of excitatory layer 2/3 neurons in mouse barrel cortex. *Front. Neuroanat.* 12:33. doi: 10.3389/fnana.2018.00033

Yao, Z., van Velthoven, C. T. J., Nguyen, T. N., Goldy, J., Sedeno-Cortes, A. E., Baftizadeh, F., et al. (2021). A taxonomy of transcriptomic cell types across the isocortex and hippocampal formation. *Cell* 184, 3222–3241.e26. doi: 10.1016/j.cell.2021.04.021

Zeng, H., and Sanes, J. R. (2017). Neuronal cell-type classification: challenges, opportunities and the path forward. *Nat. Rev. Neurosci.* 18, 530–546. doi: 10.1038/nrn.2017.85